Available online at
http://www.ibnusina.utm.my/jfs

Journal of Fundamental Sciences

Article

g-Jitter induced free convection boundary layer on heat transfer from a sphere with constant heat flux

Sharidan Shafie*, Norsarahaida Amin

Mathematics Department, Faculty Of Sciences, Universiti Teknologi Malaysia, 81310 UTM Skudai, Johor, Malaysia
**To whom correspondence should be addressed. E-mail: sharidan@mel.fs.utm.my*

Received 10 November 2005

ABSTRACT

The free convection from a sphere, which is subjected to a constant surface heat flux in the presence of g-jitter is theoretically investigated in this paper. The governing equations of motion are first non-dimensionalized and the resulting equations obtained after the introduction of vorticity are solved numerically using an implicit finite difference method for a limiting case Re >> 1 or the boundary layer approximations. Table and graphical results for the skin friction and wall temperature distributions as well as for the velocity and temperature profiles are presented and discussed for various parametric physical conditions Prandtl number, Pr=0.72, 1 and 7. Results indicate that g-jitter induced convective flows is stronger when Pr is small.

| g-Jitter | Free convection | Heat transfer | Boundary layer | Keller Box method |

1. Introduction

Recently, there has been a great deal of interest in the study of the effect of complex body forces and fluid motion and heat transfer. The resulting buoyancy forces, which are produced by the interaction of density gradients with the acceleration field have a complex spatio -temporal structure depending on both the nature of density gradients and spatial and frequency distributions of the vibration- induced acceleration field. The effect of such forces on fluid motion is known as gravity modulation or g-jitter induced flow and it comes from crew motions, mechanical vibrations (pump, motors, excitations of natural frequencies of space craft structure), atmospheric drag, solar drag, earth's gravity gradient and other sources. An extensive overview of these and other sources of unsteady gravitational accelerations, derived from estimates based on measurements in the space lab engineering model, have been documented by Gresho and Sani [1], and in the book by Antar and Nuotio-Antar [2]. Natural convection flow due to temperature gradient and gravity is known to have a profound effect on the homogeneous melt growth of semiconductor or metal crystals on earth-bound conditions. In low-gravity or microgravity environments, one can expect that reduction or elimination of natural convection may enhance the properties and performance of materials such as crystals. However, aboard orbiting spacecrafts all objects experience low-amplitude broadband perturbed accelerations, or g-jitter. Therefore, there is growing interest in understanding the effects of these perturbations on the system's behaviour.

Studies on g-jitter induced flows have been made by many researchers. Amin [3] has studied the heat transfer from an isothermal sphere immersed in an infinite viscous and incompressible fluid in a zero gravity environment under the influence of g-jitter. It has been shown that heat transfer is negligibly small for high-frequency g-jitter but under special circumstances, when the Prandtl number is sufficiently high, low frequency g-jitter may play an important role. Since the paper by Amin [3], many authors have investigated the effects of g-jitter on fluid motion of a viscous fluid in cavities and channels, e.g. Gershuni and Zhukorvitskiy [4], Wadih and Roux [5], Biringen and Peltier [6], Biringen and Danabasoglu [7], Alexander et.al. [8], Farooq and Homsy [9,10], Li [11,12], Pan and Li [13], Suresh et. al [14], Hirata et. al [15] and Chamka [16]. There are also three recent papers by Rees and Pop [17-19] on g-jitter effects on the free convection flow, in a porous medium [17,18] and, in a viscous (non-porous) fluid [19].

In this paper, the behaviour of g-jitter induced free convection boundary layer in microgravity from a sphere subjected to a constant heat flux is studied. Constant heat flux is considered in our studies because an important practical and experimental circumstance in many convective flows is that generated adjacent to a sphere dissipating heat uniformly. It should be mentioned that the paper by Amin [13] is for a sphere with a uniform temperature or isothermal sphere.

2. Basic Equations

Consider the buoyancy-driven laminar flow around a fixed sphere of radius a immersed in a viscous and incompressible Boussinesq fluid, which is at uniform temperature T_∞ . We assume that the sphere is placed in a fluctuating gravitational field $g^*(t^*)\boldsymbol{k}$, where $\boldsymbol{k}$ is the unit vector pointing vertically upward and we assume that $g^*(t^*) = g_0 \cos(\omega^* t^*)$, where g_0 is the magnitude of the g-jitter and ω is the frequency of the g-jitter oscillation. It is also assumed that the sphere is subjected to a constant heat flux q_w . The g-jitter induced free convection is described by the continuity, Navier-Stokes and energy equations, which can be written in non-dimensional forms as, see Amin [3],

$$\nabla . \boldsymbol{v} = 0 \tag{1}$$

$$\frac{\partial \boldsymbol{v}}{\partial t} + \varepsilon (\boldsymbol{v}.\nabla)\boldsymbol{v} = -\nabla p + \frac{\varepsilon}{Re}\nabla^2 \boldsymbol{v} + (T\cos t)\boldsymbol{k} \tag{2}$$

$$\frac{\partial T}{\partial t} + \varepsilon (\boldsymbol{v}.\nabla) T = \frac{\varepsilon}{Pr\, Re}\nabla^2 T \tag{3}$$

where t is the non-dimensional time, $\boldsymbol{v}$ is the non-dimensional velocity vector, T is the non-dimensional fluid temperature and p is the non-dimensional pressure. These quantities are defined as

$$t = \omega^* t^*,\ r = r^*/a,\ v = v^*/U_c,\ T = (T^* - T_\infty)/(aq_w/\kappa)$$
$$p = (p^* - p_\infty)/(\rho a \omega^* U_c) \tag{4}$$

Further, U_c is the characteristic velocity, Re is the Reynolds number and ε is a dimensionless parameter given by

$$U_c = g_0 \quad \beta \quad (a \quad q_w/k)/ \quad \omega^*,\ R \quad e = U_c \quad a/\upsilon,\ \varepsilon = U_c/a \quad \omega^* \tag{5}$$

with k being the thermal conductivity and υ is the kinematic viscosity. We note that ε is a measure of the ratio of the amplitude of fluid particles fluctuations to the radius of the sphere and, as we can see below, *Re* is interpreted as a Reynolds number which characterizes the induced steady streaming. We remark that this Reynolds number is larger by a factor ε^{-1}. Note that ε^{-1} is the Strouhal number and the familiar Grashof number is related to ε, *Re* as $Gr = \dfrac{\mathrm{Re}^2}{\varepsilon}$.

It is convenient to eliminate the pressure from (2), and introduce the vorticity $\boldsymbol{\omega}$ which then satisfies

$$\frac{\partial \boldsymbol{\omega}}{\partial t} - \varepsilon \nabla \times \left(\boldsymbol{v} \times \boldsymbol{\omega} \right) = \frac{\varepsilon}{R} \nabla^2 \boldsymbol{\omega} + \nabla \times T \cos t \boldsymbol{k} \tag{6}$$

With reference to spherical polar coordinates (r, θ, ϕ) with θ corresponding to the direction of $\boldsymbol{k}$, we have for axisymmetric flow, $\boldsymbol{v} = (v_r, v_\theta, 0)$ and $\boldsymbol{\omega} = (0, 0, \omega)$. We define a stream function ψ such that the velocity components v_r, v_θ and the stream function are related by

$$v_r = \frac{1}{r^2 \sin\theta} \frac{\partial \psi}{\partial \theta}, \; v_\theta = - \frac{1}{r \sin\theta} \frac{\partial \psi}{\partial r} \tag{7}$$

$$\omega = - \frac{D^2 \psi}{r^2 \sin\theta_a} \tag{8}$$

Equation (1) is then satisfied identically and the vorticity equation (6) and the energy equation (3) may be written in non-dimensionalized form as

$$\frac{\partial}{\partial t}(D^2 \psi) + \varepsilon \left\{ \frac{1}{r^2} \frac{\partial (\psi, D^2 \psi)}{\partial (r, \mu)} + \frac{2}{r^2} D^2 \psi L_1 \psi \right\} = \frac{\varepsilon}{Re} D^4 \psi + (1 - \mu^2)(L_2 T) \cos t \tag{9}$$

$$\frac{\partial T}{\partial t} + \frac{\varepsilon}{r^2} \frac{\partial (\psi, T)}{\partial (r, \mu)} = \frac{\varepsilon}{RePr} (D^2 T + \frac{2}{r^2} L_2 T) \tag{10}$$

where in (9) and (10)

$$D^2 = \frac{\partial^2}{\partial r^2} + \frac{(1 - \mu^2)}{r^2} \frac{\partial^2}{\partial \mu^2}, \; L_1 = \frac{\mu}{1 - \mu^2} \frac{\partial}{\partial r} + \frac{1}{r} \frac{\partial}{\partial \mu}, \; L_2 = r \frac{\partial}{\partial r} - \mu \frac{\partial}{\partial \mu}$$

and $\mu = \cos\theta$. We shall solve these equations assuming the following boundary conditions

$$\psi = \frac{\partial \psi}{\partial r} = 0 \quad \text{on} \quad r = 1 \tag{11}$$

$$\psi = \mathrm{o}(r^2) \quad \text{as} \quad r \to \infty \tag{12}$$

$$\frac{\partial T}{\partial r} = -1 \quad \text{on} \quad r = 1 \tag{13}$$

$$T \to 0 \quad \text{as} \quad r \to \infty \tag{14}$$

3. Solution Procedure

Fluids with a very large Prandtl number, *Pr*, anticipate that even small steady streaming velocities may enable convective heat transfer to overwhelm that due to pure diffusion. We now address this situation by assuming *Re*=O(1) and *Pr*=O(1) where convective effects are important, and we anticipate that the time-averaged temperature at leading order will not be of the purely diffusive form (see equation (37) in Sharidan et. al. [20]). Following Amin [3] we develop the solutions for case Re >> 1 by substitute expansion

$$\psi = \psi_0 + (\frac{\varepsilon}{Re})^{1/2}\ \psi_1 + (\frac{\varepsilon}{Re})\psi_2 + ..., \tag{15}$$

$$T = T_0 + (\frac{\varepsilon}{Re})^{1/2}\ T_1 + (\frac{\varepsilon}{Re})T_2 + ..., \tag{16}$$

into (9) and (10). Before embarking upon our solution procedure in detail, we remark that the main aim of our investigation is to determine the behaviour of the time-averaged heat transfer at the surface of the sphere, that is $\psi_0^{(s)}$ and $T_0^{(s)}$. Therefore the equations satisfied by $\psi_0^{(s)}$ and $T_0^{(s)}$ are given by

$$\frac{1}{Re}D^4\psi_0 - \left\{\frac{1}{r^2}\frac{\partial(\psi_0^{(s)}, D^2\psi_0^{(s)})}{\partial(r,\mu)} + \frac{2}{r^2}D^2\psi_0^{(s)}L_1\psi_0^{(s)}\right\} \tag{17}$$

$$= \frac{1}{r^2}\ \frac{\partial(\psi_0^{(u)}, D^2\psi_0^{(u)})}{\partial(r,\mu)} + \frac{2}{r^2}D^2\psi_0^{(u)}L_1\psi_0^{(u)} - \frac{(1-\mu^2)}{Re}(L_2T_2^{(u)})\cos t \tag{18}$$

$$\frac{1}{Pr}\left(D^2T_0^{(s)} + \frac{2}{r^2}\ L_2T_0^{(s)}\right) = \frac{Re}{r^2}\frac{\partial(\psi_0^{(s)},\ T_0^{(s)})}{\partial(r,\ \mu)} \tag{19}$$

Whereas the equations for $\psi_0^{(u)}$ and $T_0^{(u)}$ are given by

$$\begin{aligned}\frac{\partial}{\partial t}(D^2\psi_0^{(u)}) &= (1-\mu^2)(L_2T_0^{(s)})\ \cos t\\ \frac{\partial T_2^{(u)}}{\partial t} &= -\ \frac{Re}{r^2}\frac{\partial(\psi_o^{(u)}, T_0^{(s)})}{\partial(r,\mu)}\end{aligned} \tag{20}$$

We consider now the limiting case when $Re \to \infty$, or boundary layer approximation. This boundary layer has the thickness $O(Re^{-1/3})$ that encompasses the much thinner Stokes layer for *Re* << 1. It is also worth mentioning that for the corresponding isothermal sphere problem, the thickness of the boundary layer is $O(Re^{-1/2})$ and it shows clearly the difference between the two problems. The variables appropriate to this boundary layer region are

$$\psi = Re^{-2/3}\overline{\psi}(t,\mu,\overline{\eta}),\ T = Re^{-1/3}\overline{\Im}(t,\mu,\overline{\eta}),\ r-1 = Re^{-1/3}\overline{\eta} \tag{21}$$

Substituting (21) into equations (17) to (20) and letting $Re \to \infty$, we obtain the following boundary layer equations for the corresponding functions $\overline{\psi}_0^{(s)}, \overline{\psi}_0^{(u)}, \overline{\Im}_2^{(u)}$ and $\overline{\Im}_0^{(s)}$ a due to g-jitter flow

$$\frac{\partial^2 \overline{\psi}_0^{(u)}}{\partial \overline{\eta}^2} = (1-\mu^2)\frac{\partial \overline{\Im}_0^{(s)}}{\partial \overline{\eta}} \quad \sin t \tag{22}$$

$$\begin{aligned} &\frac{\partial^4 \overline{\psi}_0^{(s)}}{\partial \overline{\eta}^4} - \frac{\partial(\overline{\psi}_0^{(s)},\ \partial^2 \overline{\psi}_0^{(s)}/\partial \overline{\eta}^2)}{\partial\ (\overline{\eta},\mu)} - \frac{2\mu}{1-\mu^2}\frac{\partial^2 \overline{\psi}_0^{(s)}}{\partial \overline{\eta}^2}\frac{\partial \overline{\psi}_0^{(s)}}{\partial \overline{\eta}} \\ &= \frac{\partial(\overline{\psi}_0^{(u)},\ \partial^2 \overline{\psi}_0^{(u)}/\partial \overline{\eta}^2)}{\partial(\overline{\eta},\mu)}\Bigg|^{(s)} + \frac{2\mu}{1-\mu^2}\frac{\partial^2 \overline{\psi}_0^{(u)}}{\partial \overline{\eta}^2}\frac{\partial \overline{\psi}_0^{(u)}}{\partial \overline{\eta}}\Bigg|^{(s)} - \frac{(1-\mu^2)}{Re}\cos t\,\frac{\partial \overline{\Im}_2^{(u)}}{\partial \overline{\eta}}\Bigg|^{(s)} \end{aligned} \tag{23}$$

$$\frac{\partial \overline{\Im}_2^{(u)}}{\partial t} = -Re\ \ \frac{\partial(\overline{\psi}_0^{(u)}, \overline{\Im}_0^{(s)})}{\partial(\overline{\eta},\mu)} \tag{24}$$

$$\frac{1}{Pr}\frac{\partial^2 \overline{\Im}_0^{(s)}}{\partial \overline{\eta}^2} = \frac{\partial(\overline{\psi}_0^{(s)}, \overline{\Im}_0^{(s)})}{\partial(\overline{\eta},\mu)} \tag{25}$$

To obtain an equation for the steady stream function $\overline{\psi}_0^{(s)}$, we eliminate $\overline{\psi}_0^{(u)}$ and $\overline{\Im}_2^{(u)}$ from equations (22) to (24) as follows. Equation (22) is integrated twice with respect to $\overline{\eta}$ to give

$$\overline{\psi}_0^{(u)} = (1-\mu^2)\sin t \int_0^{\overline{\eta}} \overline{\Im}_0^{(s)}(x,\mu)\ \ dx \tag{26}$$

Substituting this relation into equation (24), followed by integration with respect to *t*, we obtain

$$\frac{(\cos t)^{-1}}{Re^{2/3}}\overline{\Im}_2^{(u)} = (1-\mu^2)\overline{\Im}_0^{(s)}\frac{\partial \overline{\Im}_0^{(s)}}{\partial \mu} + 2\mu\ \ \frac{\partial \overline{\Im}_0^{(s)}}{\partial \overline{\eta}}\ \int_0^{\overline{\eta}} \overline{\Im}_0^{(s)}(x,\ \mu)dx - (1-\mu^2)\frac{\partial \overline{\Im}_0^{(s)}}{\partial \overline{\eta}}\int_0^{\overline{\eta}} \frac{\partial \overline{\Im}_0^{(s)}}{\partial \mu}(x,\mu)\ \ dx \tag{27}$$

We now integrate equation (23) once with respect to $\overline{\eta}$ and use (22), (26) and (27) to obtain the following boundary layer equation for $\overline{\psi}_0^{(s)}$

$$\frac{\partial^3 \overline{\psi}_0^{(s)}}{\partial \overline{\eta}^3} - \frac{\partial^2 \overline{\psi}_0^{(s)}}{\partial \mu \partial \overline{\eta}}\frac{\partial \overline{\psi}_0^{(s)}}{\partial \overline{\eta}} + \frac{\partial \psi_0^{(s)}}{\partial \mu}\frac{\partial^2 \overline{\psi}_0^{(s)}}{\partial \overline{\eta}^2} - \frac{\mu}{1-\mu^2}\left(\frac{\partial\ \overline{\psi}_0^{(s)}}{\partial\ \overline{\eta}}\right)^2 = -\frac{\mu}{2}(1-\mu^2)\left(\overline{\Im}_0^{(s)}\right)^2 \tag{28}$$

Equation (28) is to be solved together with (25) for the steady temperature $\overline{\Im}_0^{(s)}$ subject to the following boundary conditions.

$$\overline{\psi}_0^{(s)} = \frac{\partial \overline{\psi}_0^{(s)}}{\partial \overline{\eta}} = 0,\ \ \frac{\partial \overline{\Im}_0^{(s)}}{\partial \overline{\eta}} = -1 \ \text{ on } \ \overline{\eta} = 0 \tag{29}$$

$$\frac{\partial \bar{\psi}_0^{(s)}}{\partial \bar{\eta}} \to 0,\ \bar{\Im}_0^{(s)} \to 0 \ \text{ as } \ \bar{\eta} \to \infty \tag{30}$$

To start the numerical solution, we need to determine initial conditions of equations (28) and (25). To do it, we notice that the solution develops a singularity in the vicinity of $\mu = 1$ ($\theta = 0^0$), i.e. at the top pole of the sphere. Thus, we start the numerical solution near $\theta = 90^0$, that is, at small values of μ and expand the functions $\bar{\psi}_0^{(s)}$ and $\bar{\Im}_0^{(s)}$ in the series of small μ of the form

$$\bar{\psi}_0^{(s)} = \mu f_0(\bar{\eta}) + \mathrm{O}(\mu^3),\ \bar{\Im}_0^{(s)} = h_0(\bar{\eta}) + \mathrm{O}(\mu^2) \tag{31}$$

Substituting (39) into equations (37) and (34), we get the following ordinary differential equations for f_0 and h_0

$$f_0'''' + f_0 f_0'' - f_0'^2 = -\frac{1}{2} h_0^2,\ h_0'' + Pr f_0 h_0' = 0 \tag{32}$$

subject to the boundary conditions (38), which become

$$f_0(0) = f_0'(0) = 0,\ h_0'(0) = -1,\ f_0'(\infty) = 0,\ h_0(\infty) = 0 \tag{33}$$

where primes denote differentiation with respect to $\bar{\eta}$.

4. Method of Solution

Equations (28) and (25) subject to boundary conditions (29) to (30) were solved numerically using a very efficient finite difference scheme. The scheme employed is the box method developed by Keller [21]. This method has been shown to be particularly accurate for parabolic problems. It is faster, easier to program and it is chosen because it seems to be the most flexible of the common methods, being easily adaptable to solving equations of any order. The Keller-box method is essentially an implicit finite difference scheme, which has been found to be very suitable in dealing with nonlinear problems. Details of the method may be found in many recent publications, and here we have used the procedure outlined in Cebeci and Bradshaw [22]. One of the basic ideas of the box method is to write the governing system of equations in the form of a first order system. For this purpose, we introduce new dependent variables $y_1(\mu,\eta)$, $y_2(\mu,\eta)$, $y_3(\mu,\eta)$, $y_4(\mu,\eta)$ and $y_4(\mu,\eta)$. Let

$$y_1 = \bar{\psi}_0^{(s)},\ y_2 = \frac{\partial \bar{\psi}_0^{(s)}}{\partial \bar{\eta}},\ y_3 = \frac{\partial^2 \bar{\psi}_0^{(s)}}{\partial \bar{\eta}^2},\ y_4 = \bar{\Im}_0^{(s)},\ y_5 = \frac{\partial \bar{\Im}_0^{(s)}}{\partial \bar{\eta}} \tag{34}$$

This means that

$$y_1' - y_2 = 0 \tag{35}$$
$$y_2' - y_3 = 0 \tag{36}$$
$$y_4' - y_5 = 0 \tag{37}$$

Using (34), equations (28) and (25), then take the form

$$y_1' - y_2 = 0 \tag{38}$$

$$y_2' - y_3 = 0 \tag{39}$$

$$y_3' - \frac{\mu}{1-\mu^2} y_2^2 + \frac{1}{2}\mu\left(1-\mu^2\right) y_4^2 - y_2 y_{2\mu} + y_3 y_{1\mu} = 0 \tag{40}$$

$$y_4' - y_5 = 0 \tag{41}$$

$$y_5' - Pr(y_2 y_{4\mu} - y_5 y_{1\mu}) = 0 \tag{42}$$

Boundary conditions (29) and (30) becomes

$$y_1(\mu,0) = 0,\ y_2(\mu,0) = 0,\ y_5(\mu,0) + 1 = 0 \tag{43}$$

$$y_2(\mu,\infty) = 0,\quad y_4(\mu,\infty) = 0 \tag{44}$$

With the resulting first order equations, the "centered-difference" derivatives and averages at the midpoints of net rectangles and net segments are used, as they are required to get accurate finite difference equations. We consider the net rectangle on the plane and denote the net points by

$$\mu^1 = 0,\quad \mu^{i+1} = \mu^i + \delta\mu_i,\quad i = 1,2,...,N-1 \tag{45}$$

$$\eta_1 = 0,\quad \eta_{m+1} = \eta_m + \delta\eta_m,\quad m = 1,2,...,M-1,\quad \eta_M = \eta_\infty \tag{46}$$

Here i and m index points on the (μ,η) plane, and $\delta\mu_i$ and $\delta\eta_m$ defines the steplengths corresponding to the i^{th} and m^{th} intervals, respectively. Given a typical variable, y_1, say, the various quantities in (38) to (42) are approximates as follows,

$$y_{1m+1/2}^{i+1/2} \cong \frac{1}{4}\left(y_{1m}^{\,i} + y_{1m+1}^{\,i} + y_{1m}^{\,i+1} + y_{1m+1}^{\,i+1}\right) \tag{47}$$

$$y_{1\eta}\Big|_{m+1/2}^{i+1/2} \cong \frac{1}{2\delta\eta_m}\left(y_{1m+1}^{\,i} - y_{1m}^{\,i} + y_{1m+1}^{\,i+1} + y_{1m}^{\,i+1}\right) \tag{48}$$

$$y_{1\mu}\Big|_{m+1/2}^{i+1/2} \cong \frac{1}{2\delta\mu_i}\left(y_{1m}^{\,i+1} - y_{1m}^{\,i} + y_{1m+1}^{\,i+1} - y_{1m+1}^{\,i}\right) \tag{49}$$

If we substitute (47) to (49) into (38) to (42), the resulting finite difference equations are implicit and nonlinear. Newton's method is first introduced to linearize the nonlinear system of equations before a block-tridiagonal factorization scheme is employed on the coefficient matrix of the finite difference equations for all η at given μ. The solution of the linearized difference equations can be obtained in a very efficient manner by using the block-elimination method (Cebeci and Bradshaw [22]). In all the results quoted here were obtained using uniform grids in both the μ and η directions, with 1000 points in the range $0 \le \mu \le 1$ and 376 points in the range $0 \le \eta \le 15$. The convergence was deemed to have taken place when the maximum absolute pointwise change between successive iterates was 10^{-10}. The solution procedure to solve numerically equations (32) subject to boundary conditions (33) are the same as solving equations (28) and (25) as discussed above.

5. Results and Discussion

We have solved numerically the two systems of the steady-state boundary layer equations (28), (25) and (32) due to g-jitter flow for some values of the Prandtl number, *Pr* and at some positions θ around the sphere between $\theta = 0$ and $\theta = 90^0$. Figures 1 to 2 are presented for the results of the skin friction, $\frac{\partial^2 \overline{\psi}_0^{(s)}}{\partial \overline{\eta}^2}(0,\theta)$ the wall temperature, $\overline{\Im}_0^{(s)}(0,\theta)$ for the steady part of the solution induced by g-jitter for *Pr* = 0.7 (air), 1 and 7 (water at $21^0 C$).

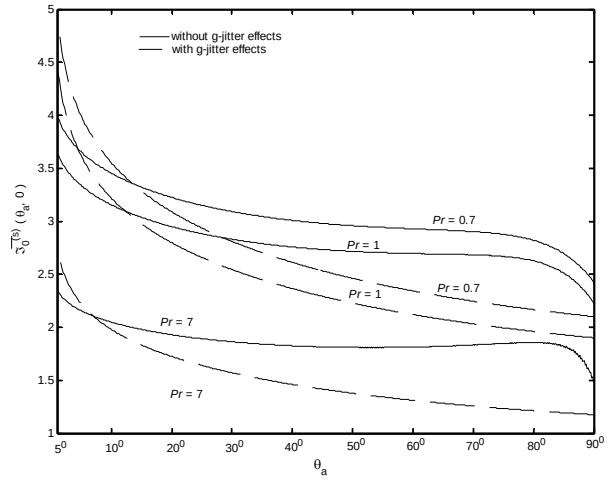

Fig. 1 Variations of the wall temperature with θ for different values of Prandtl numbers, *Pr*.

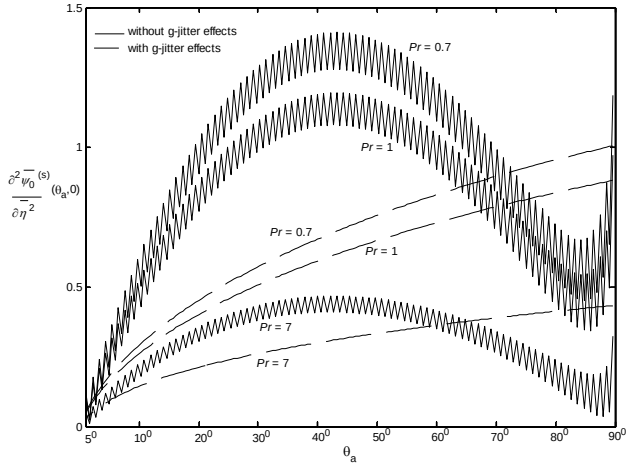

Fig. 2 Variations of the skin friction with θ for different values of Prandtl numbers, *Pr*.

Table 1 The local reduced skin friction $\frac{\partial^2 \overline{\psi}_0^{(s)}}{\partial \overline{\eta}^2}(0,\theta)$ and the local wall temperature $\overline{\Im}_0^{(s)}(0,\theta)$ at different position of θ for Pr=0.72, 1 and 7.

Pr	0.72		1		7	
θ	$\frac{\partial^2 \overline{\psi}_0^{(s)}}{\partial \overline{\eta}^2}(0,\theta)$	$\overline{\Im}_0^{(s)}(0,\theta)$	$\frac{\partial^2 \overline{\psi}_0^{(s)}}{\partial \overline{\eta}^2}(0,\theta)$	$\overline{\Im}_0^{(s)}(0,\theta)$	$\frac{\partial^2 \overline{\psi}_0^{(s)}}{\partial \overline{\eta}^2}(0,\theta)$	$\overline{\Im}_0^{(s)}(0,\theta)$
90^0	1.594242	2.395948	1.332250	2.213087	0.485758	1.469306
88^0	0.567872	2.548519	0.431899	2.377211	0.061693	1.708572
86^0	0.659330	2.597671	0.548691	2.428262	0.161067	1.754499
84^0	0.483570	2.643930	0.374212	2.475995	0.071712	1.799002
82^0	0.511158	2.767135	0.409171	2.593914	0.123893	1.849555
80^0	0.704421	2.805004	0.584361	2.626362	0.224529	1.849991
78^0	0.609979	2.831340	0.503572	2.647953	0.177638	1.850459
76^0	0.810075	2.850874	0.680843	2.662312	0.268956	1.844182
74^0	0.728309	2.864931	0.609844	2.672243	0.226146	1.840563
72^0	0.924951	2.875482	0.781754	2.679308	0.309857	1.834267
70^0	0.851906	2.884212	0.717747	2.683680	0.270668	1.828626
65^0	1.115252	2.897852	0.944885	2.690024	0.371281	1.815706
60^0	1.101062	2.909168	0.930450	2.695749	0.352301	1.808018
45^0	1.281562	2.959384	1.082977	2.733195	0.409876	1.809939
30^0	1.167679	3.069436	0.989695	2.829819	0.380642	1.857472
20^0	0.905724	3.202942	0.771468	2.950161	0.305125	1.924321
10^0	0.603268	3.429099	0.518102	3.155808	0.220308	2.042462
1^0	0.113513	3.950262	0.098046	3.633329	0.045350	2.328067

Figures 1 to 2 show the comparison of the non-dimensional skin friction and wall temperature between the g-jitter case and without g-jitter case (Nazar et. al. [23]). It is shown that the skin friction for the g-jitter effect has an oscillation behaviour. However, the oscillation behaviour for the wall temperature for g-jitter case is very small. Both skin friction and wall temperature are larger for the g-jitter case than that for the case without g-jitter effect. However, as θ increases starting from $\theta = 60^0$, the skin friction for g-jitter case is smaller than that without g-jitter effects case, but, then near $\theta = 90^0$ the skin friction for g-jitter case is drastically increases.

For the case of g-jitter effects, Figures 1 to 2 show that the surface temperature decreases almost continuously from the value at the upper pole ($\theta = 0^0$) to a finite value at $\theta = 90^0$. However, the skin friction is first increases from the upper pole $\theta = 0^0$ to a maximum value, then it decreases to a minimum value and then it

increases indefinitely, at $\theta = 90^0$ The peak of these profiles decreases as the values of *Pr* decreases. This behavior may be attributed due to the g-jitter effects. Some values of the non-dimensional skin friction and non-dimensional surface temperature are given in Table 1 for *Pr* = 0.7, 1 and 7, and several values of the angle θ. It is seen that the skin friction along the sphere increases as θ increases, as expected, and it has an oscillatory behavior. However the surface temperature decreases with the increase in θ. It is also seen that both the skin friction and the surface temperature decrease as the Prandtl number *Pr* increases.

It is worth mentioning that such a singularity at the pole has been observed also by Potter and Riley [24] and Brown and Simpson [25] for the same boundary layer problem without g-jitter effect. Latter, Omar Awang [26] was able to extend the range of the calculations almost to the upper pole of the sphere. He also demonstrated that the analytical structure close to upper pole derived by Brown and Simpson [25] is consistent with his numerical solution.

6. Conclusion

The secondary steady motion, or acoustic streaming, consists of a momentum (velocity) and a thermal boundary layer, and the solution of the corresponding boundary layer equations is determined numerically using the Keller-box method. It is found that the skin friction increases indefinitely at the pole of the sphere $\theta = 0^0$, while the wall temperature remains finite at this point. It is worth mentioning that the solution presented here may also prove useful as a guide for more complex g-jitter accelerations such as, for example, a sum of Fourier harmonic components with distinct frequencies and amplitudes considered by Li [11]. It is hoped that the solution presented here, as well as in Amin [3], will further serve as a foundation for more complex and realistic studies of free and mixed convection flows from bodies of other configurations and also under the influence of an external magnetic field. It will also help to develop baselines for practical microgravity processing system design and development.

7. Acknowledgement

The authors wish to thank to Prof. Ioan Pop for his generous guidance while he visited Universiti Teknologi Malaysia, in 2005.

8. References

[1] P. M. Gresho, R. L. Sani, J. Fluid Mech, 40 (1970) 783-806.
[2] B. N. Antar, V. S. Nuotio-Antar, Fundamental of Low Gravity Fluid Dynamics and Heat Transfer. Boca Raton: CRC Press. 1993.
[3] N. Amin, Proc. R. Soc. Lond., A 419 (1988) 151-172.
[4] G. Z. Gershuni, M. Y. Zhukorvitskiy, Fluid Mech.- Sov. Res., 15 (1986) 63-84.
[5] M. Wadih, R. J. Roux, J. Fluid Mech., 193 (1988) 391-415.
[6] S. Biringen, L. J. Peltier, Phys Fluids, A 2 (1990) 279-283.
[7] S. Biringen, A. I. A. A. Danabasoglu, Thermophys heat transfer, 4 (1990) 357-365.
[8] J. I. D. Alexander, S. Amirondine, J. Ouzzani, F. J. Rosenberger, J. Cryst Growth, 113 (1990) 21-38.
[9] A. Farooq, G. M. Homsy, J. Fluid Mech., 271 (1994) 351-378.
[10] A. Farooq, G. M. Homsy, J Fluid Mech., 313 (1996) 1-38.
[11] B. G Li, Int. of Heat and Mass Transfer, 39 (1996) 2853-2890.
[12] B. G. Li, Int. J. Eng. Sci., 34 (1996) 1369-1383.
[13] B. P. Pan, B. G. Li, Int. J. Heat Mass Transfer, 17 (1998) 2705-2710.

[14] V. A. Suresh, C. A. Christov, G. M. Homsy, Phys. Fluids 11 (1999) 2585-2576.
[15] K. Hirata, T. Sasaki, H. Tanigawa, J. Fluid Mech., 445 (2001) 327-334.
[16] A. J. Chamkha, Heat Mass Transfer, 39 (2003) 553-560.
[17] D. A. S. Rees, I. Pop, Int. Comm. Heat Mass Transfer , 27 (2000) 415-424.
[18] D. A. S. Rees, I. Pop, Int. of Heat and Mass Transfer, 44 (2001) 877-883.
[19] D. A. S. Rees, I. Pop, Heat and Mass Transfer, 37 (2001) 403-408.
[20] S. Sharidan, N. Amin, I. Pop, International Journal of Heat and Mass Transfer, 2005. (Accepted)
[21] H. B. Keller, A new difference scheme for parabolic problems, in numerical solutions of partial differential equations (B.Hubbard, ed)}. New York: Academic Press. 2: 327-350, 1971.
[22] T. Cebeci, P. Bradshaw, Physical and Computational Aspects of Convective Heat Transfer, New York: Springer, 1984.
[23] R. Nazar, N. Amin, I. Pop, International Communications in Heat and Mass Transfer, 29 (2002) 1129 - 1138.
[24] J. M. Potter, N. Riley, J. Fluid Mech., 100 (1980) 769-783.
[25] S. N. Brown, C. J. Simpson, J. Fluid Mech., 124 (1982) 123-137.
[26] M. A. Omar Awang,, J. Math. Phy. Sci., 18 (1984) S115 - S125.